Iranian Journal of Oil & Gas Science and Technology, Vol. 2 (2013), No. 1, pp. 42-56
http://ijogst.put.ac.ir

A Novel Combinatorial Approach to Discrete Fracture Network Modeling in Heterogeneous Media

S. Balouchi[1], S. Moradi[1*], M. Masihi[2], and A. Erfaninia[3]

[1] Department of Petroleum Exploration, Petroleum University of Technology, Abadan, Iran
[2] Department of Chemical and Petroleum Engineering, Sharif University of Technology, Tehran, Iran
[3] National Iranian South Oil Company, Ahwaz, Iran

Abstract

Fractured reservoirs contain about 85 and 90 percent of oil and gas resources respectively in Iran. A comprehensive study and investigation of fractures as the main factor affecting fluid flow or perhaps barrier seems necessary for reservoir development studies. High degrees of heterogeneity and sparseness of data have incapacitated conventional deterministic methods in fracture network modeling. Recently, simulated annealing (SA) has been applied to generate stochastic realizations of spatially correlated fracture networks by assuming that the elastic energy of fractures follows Boltzmann distribution. Although SA honors local variability, the objective function of geometrical fracture modeling is defined for homogeneous conditions. In this study, after the introduction of SA and the derivation of the energy function, a novel technique is presented to adjust the model with highly heterogeneous data for a fractured field from the southwest of Iran. To this end, the regular object-based model is combined with a grid-based technique to cover the heterogeneity of reservoir properties. The original SA algorithm is also modified by being constrained in different directions and weighting the energy function to make it appropriate for heterogeneous conditions. The simulation results of the presented approach are in good agreement with the observed field data.

Keywords: Discrete Fracture Network, Correlated Fracture Network, Simulated Annealing, Heterogeneous Media, Boltzmann Distribution

1. Introduction

Fractured reservoirs, because of their complex geological nature, cannot be described by conventional homogenous models. Stochastic approaches are recently employed for the proper characterization of heterogeneous fracture networks in porous media. These methods represent local variability and uncertainty and are also able to integrate both hard and soft data sources in the modeling process.
Geostatistical simulation has two major classes of pixel-based and objects-based modeling (OBM). The pixel-based technique uses multipoint statistics in a binary space (Guardiano and Srivastava, 1993) but is not applicable to large scale modeling especially in cases like fracture modeling which is used in a wide range from microcracks to major faults. Alternatively, OBM's, which utilize predefined objects carrying several properties in the matrix background, honor the shape and size distribution of a wide range of objects as individual elements (Bear et al., 1993). Compared to ordinary grid-based methods, this approach is also applicable to large systems and supports stochastic solutions. The main

* Corresponding Author:
Email: moradi.s@put.ac.ir

drawback of this class of modeling methods is the difficulty of being conditioned by real data and the incorporation of heterogeneities. Simulated annealing (SA), which is based on MCMC, is a conditioning method for defining likelihood functions to probabilistically optimize realizations from prior and subsequent configurations in an iterative algorithm. Heffer introduced a spatial correlation function of fractures as displacement strain vectors using renormalization techniques based on the idea of Daly (Daly, 2001) in the representation of stochastic tensor fields for strain modeling (Heffer and King, 2006). Masihi applied this method to generate fracture networks based on the assumption that the elastic energy in the fractured media follows a Boltzmann distribution (Masihi and King, 2007). The spatial correlation expression of fracture displacements is globally minimized by simulated annealing algorithm. SA assumes a mechanical equilibrium (Kirkpatrick et al., 1983) in a reference rock sample which is equivalent to maximum entropy and minimum energy, i.e. the best statistical correlation between the components. Shekhar applied this method to field scale fracture modeling for seismic velocity modeling in homogeneous conditions and adapted it by using outcrop observations (Shekhar and Gibson, 2008; Shekhar and Gibson, 2011). Hals investigated the correlation of fracturing process for two independent injection points in hydraulic fracturing (Hals and Berre, 2012). Masihi also applied the method to 3D fracture modeling (Masihi et al., 2012).

In this work, we first derive the spatial correlation function for discrete fracture network modeling and then discuss about SA as an optimization algorithm to minimize the predefined objective function. Next step is to integrate geological data and use them to adapt the simulation to a highly tectonized region, i.e. the southwest of Iran. To this end, formation microimager (FMI) logs are applied to detect the fracture dip and azimuth, well testing is employed to estimate the mean length, and the rock mechanic parameters of reservoir rock are collected from DSI logs. Finally, a novel technique is presented to condition the algorithm by using the heterogeneities of fractured reservoirs through combining grid-based and object-based methods in order to associate the property variation of the medium and constrain SA in x and y directions. On the other hand, for better results, rock properties and fracture intensity were incorporated in the calculations by the application of weighted energy calculation.

2. Modeling

2.1. Spatial correlation function of displacement vectors

To derive an appropriate elastic energy function for the spatial correlation of fractures with displacement vectors, elastic medium, i.e. reservoir rock, is considered, where fractures are assumed as discontinuities in the system. Fractures are indicated as a displacement vector from x to x', that is to say $u(x)=x-x'$. The strain vectors have two elastic and inelastic components of u^e and u^i respectively. Similarly, the strain and stress can be decomposed into elastic and inelastic parts:

$$\begin{aligned} \sigma_{ij} &= \sigma_{ij}^{e} + S \\ e_{ij} &= e_{ij}^{e} + E_{ij} \end{aligned} \tag{1}$$

Landau proved that stress tensor could be written in terms of the strain tensor for isotropic elastic medium via Hook's law as given below (Landau and Lifshitz, 1982b):

$$\sigma_{ij}^{e} = \lambda e_{ij}^{e} \delta_{ij} + 2\mu e_{ij}^{e} \tag{2}$$

where, the strain tensor for small deformations is given by:

$$e_{ij}^{e} = \left(\partial j u_i^e + \partial i u_j^e \right) \Big/ 2 \tag{3}$$

By the assumption of a mechanical equilibrium in the absence of external forces, continuity equation in isotropic media becomes:

$$\partial_j \sigma_{ij} = \partial_j \sigma_{ij}^e e_{ij} + \partial_j S_{ij} = 0 \tag{4}$$

or

$$\partial_j \sigma_{ij}^e e_{ij} = -\partial_j S_{ij} \tag{5}$$

It can be interpreted as the imaginary body force keeping the fracture open. The total elastic energy in terms of strain and stress is $E = \sigma_{ij}^e e_{ij}^e / 2$. By using the Fourier transform of stress and strain fields, the energy reads:

$$E(k) = \frac{1}{2}[\sigma_{ij}^e][e_{ij}^e] = \frac{1}{2}\left[i\lambda_{ijal}k_a u_l^e\right]\left[\frac{i}{2}\left(\delta_{aj}\delta_{jl} + \delta_{ai}\delta_{il}\right)k_a u_l^e\right] = \frac{\mu}{2}L_{kl}(k)u_k^e(k)u_l^e(-k) \tag{6}$$

where, standard isotropic elasticity tensor is considered as:

$$\lambda_{ijal} = \lambda\delta_{ij}\delta_{al} + \mu\left(\delta_{ia}\delta_{jl} + \delta_{il}\delta_{ja}\right) \tag{7}$$

L_{kl} is the linear operator of isotropic elasticity and is given as the inverse of the Green's function, $L_{kl}G_{lm}=\delta_{km}$. As mentioned above, we assume that the frequency distribution of the strain energy follows Boltzmann probability law:

$$P(E) \propto \exp\left(-E / \langle E \rangle\right) \tag{8}$$

It implies that fractures, or dislocations, tend to lie in maximum entropy configuration subjected to a fixed mean strain energy, i.e. $\langle E \rangle = k_b T$, where k_b is Boltzmann constant and T is temperature. By applying this hypothesis, a spatial correlation between fractures acting as the elastic displacements in a real space is given by:

$$C_{kl}(r) = \frac{\langle E \rangle}{\mu}G_{kl}(r) = \frac{\langle E \rangle}{16\pi\mu(1-\upsilon)}\left(\frac{3-4\upsilon\delta_{kl}}{r} + \frac{r_k r_l}{r^3}\right) \tag{9}$$

Heffer and King rearranged Equation 9 as follows (Heffer and King, 2006):

$$\left\langle u_i^e(r)u_j^e(-r)\right\rangle = \frac{A}{r}.\left[\eta.\delta_{ij} + \frac{r_i r_j}{r^2}\right] / r \tag{10}$$

where, δ_{ij} is the Kronecker delta and η is equal to 3-4 v; $A=\langle E \rangle/16\pi\mu(1-v)$. $\langle E \rangle$, μ, and v stand for mean strain energy, shear modulus, and the Poisson's ratio of the rock sample respectively and satisfy the continuity equation (Equation 5). The demonstration of the general class of covariance tensors and the above covariance function belongs to Daly (Daly, 2001). It can also be written in the vector form:

$$\left\langle u_i^e(r)u_j^e(-r)\right\rangle = \left[A.\frac{\eta.(u_i,u_j)}{r} + \frac{(r,u_i).(r,u_j)}{r^3}\right] \tag{11}$$

where, (u_i,u_j) is the scalar product of two vectors u_i and u_j representing two fractures or displacement vectors at points i and j with a distance vector of r. The summation of the above covariance function for all the pairs of vectors (u_i,u_j) in the system is our target function in the stochastic simulation. Equation 11 can be simplified for 2D medium as:

$$E = \sum A.u_i.u_j.\left[\eta.\left|\cos(\theta_j - \theta_i)\right| + \left|\cos(\alpha - \theta_i)\cos(\alpha - \theta_j)\right|\right] \Big/ r_{ij} = \\ = \sum A.\left[\eta.\left|u_i^x u_j^x + u_i^y u_j^y\right| + r_{ij}^{-2}.\left|(u_i^x r_{ij}^x + u_i^y r_{ij}^y)(u_j^x r_{ij}^x + u_i^y r_{ij}^y)\right|\right] \Big/ r_{ij} \quad (12)$$

where, α, θ_i, and θ_j are the orientation of distance vector r and fractures u_i and u_j with respect to the horizon respectively.

2.2. Model description

Equation 12 is applied as the objective energy function of the simulated annealing algorithm introduced by Kirkpatrick (Kirkpatrick, 1983). SA enables us to solve combinatorial optimization problems involving a large number of independent variables (Tran, 2007; Tran et al., 2006). Unlike linear optimization methods, which find the nearest minimum value to the initial state, energy function in SA converges to the global optimum. Alongside energy, a pseudo-temperature parameter, T, is also defined as a simulation controlling factor. T allows the model to escape local minima and gives it a chance to be in a high-energy state even at low temperatures (Aarts and Korst, 1989). It must be noted that E and T are not exactly thermodynamic parameters, just as their notations show.

To start the simulation, an initial configuration of fracture network is needed to be optimized by SA. The initial fracture distribution can be assumed to be uniform (random) or the outputs of some other faster simulators, according to the generality of the algorithm. The random initiation is preferred because the dislocation of large-scale features is hard to correct and random realization implies a larger space of uncertainty, which results in more realistic realizations (Deutsch, 2002).

Subsequently, a perturbation mechanism should be defined to consider small stochastic changes in the properties of the objects. In each perturbation, the energy is recalculated to check if it decreases or not. If the energy falls, it means that the annealing process is taking place, we are approaching the desired configuration, and the change is accepted. However, if it rises, the acceptance of the perturbation depends on Metropolis algorithm (Metropolis et al., 1953) proportional to Boltzmann factor ($e^{-\Delta E/T}$) probability. In other words, the acceptance probability is calculated by $P_{accept}=min\{1, e^{-\Delta E/T}\}$ and compared with a random number in the close interval of [0,1] to prevent trapping in a local minima. Moreover, initial T must be high enough to allow energy to freely change and it is recommended that T should be set in the same order of magnitude as E. While a set of perturbations proportional to the number of objects is implemented and the new energy state is measured, the ratio of the number of accepted changes to total perturbation forms is calculated as an acceptance ratio.

After a set of perturbations, temperature must decrease. A schedule for T reduction as $T_{i+1}=\alpha T_i$ is defined, where α is assumed to be 0.97 in this work. In the initial steps, the acceptance ratio (the number of accepted changes per all the perturbations) must be over 95 percent for reliable results. However, this ratio decreases along the annealing process to hold steady at a certain value which is the desired realization. The stopping criterion of the simulation is accepting less than 1 percent of the perturbations. Figure 1 briefly displays the flowchart of the SA algorithm used for fracture network modeling.

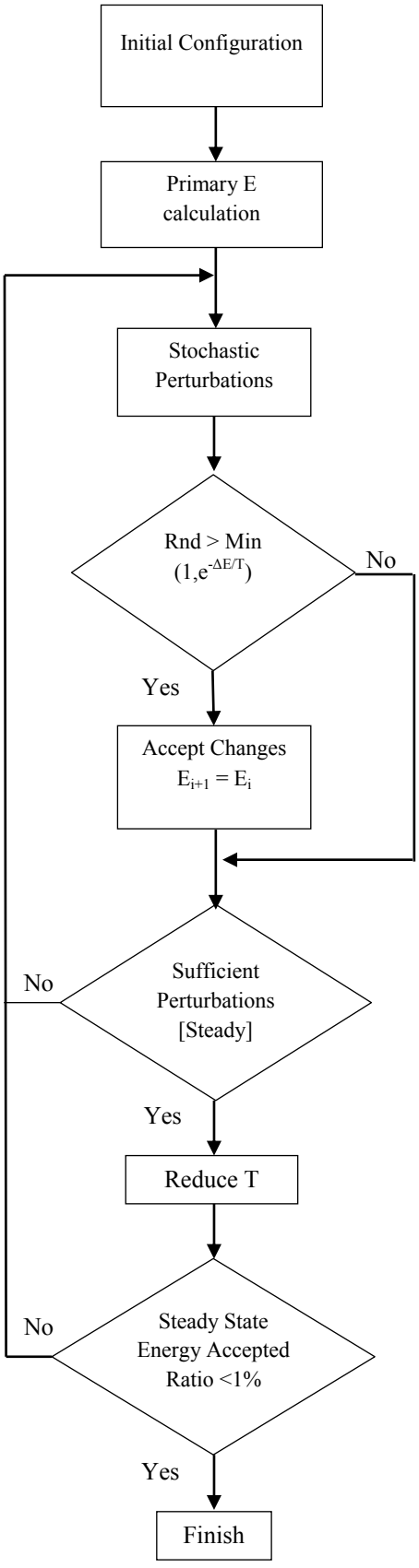

Figure 1
Simple simulated annealing flowchart for global optimization

We consider a 2D medium as the simulation area and fractures as strain displacement vectors with a length of l, an orientation of θ, and a location vector of r from the origin of coordinates to the center of each fracture, randomly distributed through the medium. Perturbation mechanisms are applied iteratively to randomly selected fractures. To produce a sufficient number of perturbations that allow the objects to vary freely and converge to the global minimum of energy state, averagely ten perturbations are assigned to each fracture per every T-step as given below:

$$\theta_i^{new} = \theta_i^{old} + 0.03\pi \times (2Rnd - 1) \tag{13-1}$$

$$l_i^{new} = l_i^{old} + 0.1 \times (2Rnd - 1) \tag{13-2}$$

$$r_i^{new} = r_i^{old} + 0.1 \times (2Rnd - 1) \tag{13-3}$$

where, Rnd is a random number from a uniform distribution in the close interval of [0, 1].
During the annealing process, the first cosine term of the energy function in Equation 12 tends to set the fractures in an orthogonal situation while the second combined cosine term tends to set them parallel. The η coefficient applies appropriate weight to the first term and determines whether fractures lie in perpendicular or parallel sets. η is calculated from Poisson's ratio and depends on the rock properties. Masihi and King accomplished a sensitivity analysis on η values and found out that negative values preferred to generate one single parallel set whereas positive values showed two perpendicular fractures sets (Masihi and King, 2007). Typical values of v for subsurface rocks are between 0.2 and 0.3 (Engedler and Peacock, 2001), which implies frequently occurring orthogonal sets of fractures.
It must be noted that a finite size model in SA with the truncation of boundaries or the limitation of stress field is considered herein. This truncation implies that fractures on the boundaries experience lower stress compared to the others and cause artifacts in the final results. To overcome this problem, a periodic boundary condition is applied; in other words, same modeling medium is considered next to the boundaries in all directions. As a result, the fractures located on the boundaries have their own pairs with the same properties on the opposite side, which neutralized the boundary effect.

2.3. Geological setting

The variation of tectonic forces in the southwest of Iran has caused extreme stress heterogeneities. The folding and faulting through orogeny processes have also intensified the problem. In folding, the convex side is thinned and subjected to tension, hence normal faults may occur there; on the other hand, the concave side is thickened and subjected to compressional forces, thus generating reverse faults. Therefore, different rock mechanical parameters in the vertical direction and obviously different fracture densities are expected (Singhal and Gupta, 2010).

a. Formation microimager (FMI) logging to determine fracture density

Formation microimager loges are a proper tool for detecting formation discontinuities such as bedding surface or cracks. The results of FMI logs of two wells in both sides of the modeling area indicate that there are no fractures in the upper middle part of the formation due to a low strain (neutral plane of fold) and high rock elasticity. The maximum intensity of fractures is occurred in lower extremes (especially in Well #1) due to faulting and high compressional forces, which is categorized as strongly fractured in Ruhland's classification (Ruhland, 1973); The other zones experience a practical to average fracturing degree in the same classification. In addition to vertical heterogeneity, the results

also show lateral heterogeneity; that is to say that the trend of the variations in Well #1 is not supported by the second well, Well #2 (See Table 1).

Table 1
Fracture intensity and density in Wells 1 and 2; zone 4 experiences no fractures

		Well #1			Well #2		
Zone	**Thickness**	**Count**	**Intensity**	**AD**	**Count**	**Intensity**	**AD**
1	43	1	0.022472	0.061901	3	0.069767	0.110571
2	46	9	0.204545	0.244711	20	0.434783	0.892417
3	76	0	0	0	5	0.065789	0.092732
4	98	0	0	0	0	0	0
5	59	0	0	0	16	0.271186	0.647295
6	181	5	0.030675	0.043846	9	0.05	0.10253
7	47	205	4.1	4.973084	7	0.155556	0.25984

Fracture areal density is defined as the summation of length of fractures divided by cross sectional area for reservoir simulation aims. A sampling bias, which is inversely proportional to the cosine of the acute angle between the borehole axis and the fracture pole, is introduced by Terzaghi (Terzaghi, 1965). However, the introduced weight factor approaches infinity where fracture pole is at a steep angle with respect to the wellbore direction. Priest modified the method to reduce the effect of skewing the weighted data by setting a maximum allowable weighting of 10 (Priest, 1993). Table 1 briefly shows the intensity and areal density of each zone by implementing the above corrections.

b. Transient well testing analysis to determine fracture lengths

To convert the areal density to individual fractures, the mean length of fractures is needed. This could be achieved by outcrop studies or transient well testing interpretation; however, because the outcrop studies may be accomplished kilometers far from the reservoir location and can be subjected to weathering and different stresses, they are not suitable for such a region. Alternatively, Warren and Root introduced a primary sugar cube dual porosity model by using well tests (Warren and Root, 1963), which was later extended by Belani et al. to determine block sizes from pressure responses (Belani et al., 1988). Block size can be calculated for slabs, cylindrical, or cubic models. Because the value of η is between 1.9 and 2 herein, as will be indicated in further calculations, we face two sets of fractures. Hence, a cubic or spherical model is used in the calculation of block sizes, i.e. n=3 in $\alpha = \frac{n(n+2)}{r_m^2}$, where r_m is the characteristic size of the block (Bourdet, 2002). The average value of r_m is found to be 174.66 ft (53.236 m), which stands as fracture mean length where matrix permeability is considered about 1 *md*. By the estimation of mean length and areal densities, one can find out how many fractures will occur in the medium. Contrary to primary continuum models, this length does not remain constant and varies due to fracture intensity and density in different directions. Therefore, the simulation deduces a distribution of fracture length instead of a single length in the whole media.

c. DSI logging for rock mechanical properties

Another important stage of fracture modeling is rock mechanics studies. To obtain the rock modulus, the propagation of acoustic waves in the formation is applied. DSI logs provide us with the transit time of compressional, shear, and stoneley waves. Shear modulus could be calculated by:

$$\mu = \frac{a\rho_b}{DTS^2} \tag{14}$$

where, a=1.34×10^{10} and Poisson's ratio is defined by:

$$PR = \frac{\frac{1}{2}\left[\frac{DTS}{DTC}\right]^2 - 1}{\left[\frac{DTS}{DTC}\right]^2 - 1} \tag{15}$$

To incorporate the heterogeneities of rock mechanical parameters in the energy calculation of each fracture pair, the geometrical averaging of two values depending on fracture locations are used instead of the global values of A and η. Figure 2 shows the variation of these parameters in the formation. For simplicity, a value of A equal to 1 is used for homogeneous bodies whereas it gradually varies in heterogeneous media.

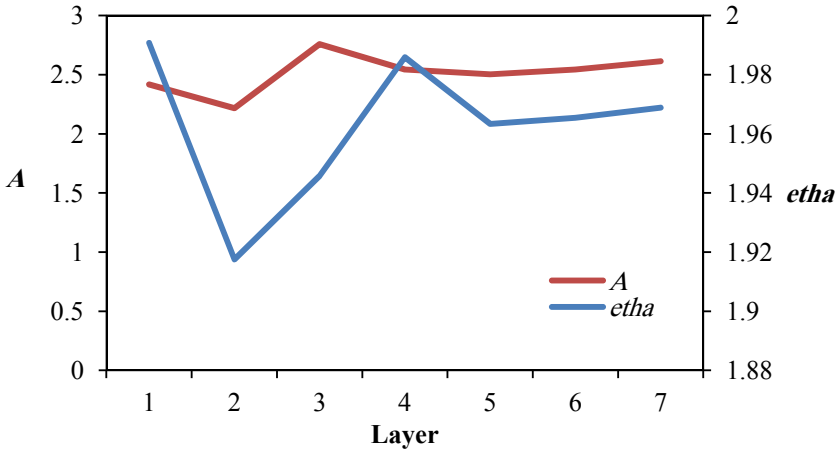

Figure 2
Variations of A and *etha* in the formation; relatively low values in zones 2 and 5 caused high densities especially in Well #2

2.4. Conditioning model with heterogeneous data

a. Combination of object-based modeling with grid-based technique

The selected region for modeling suffers from high degrees of heterogeneities in vertical and lateral directions as discussed above. 220 and 60 fractures are detected in the first and the second wells respectively. The FMI results provide the location and orientation of the fractures; subsequently, the calculated mean trace length is assigned to them in the simulation terminology. 4720 randomly distributed fractures with a normal distribution on length N (60, 2) are also uniformly distributed to stochastically cover the unknown area bounded by the wells, i.e. totally 5000 fractures with respect to average density and length.

To condition such stochastic fractures with deterministic ones, the characterized fractures will contribute in energy calculation but not in perturbation, while all stochastic fractures would be perturbed. In each iteration, the new energy state calculated from changing one property of stochastic fractures determines the correlation of new configuration with the fixed deterministic ones. This is the main framework of conditioning (especially in homogenous cases) to set the stochastic fractures in the best pattern correlated with borehole fractures during energy reduction.

Energy (Equation 12) strongly depends on fracture length as the size of displacement. So it can be deduced that the main factor reducing energy is the minimization of fracture length. Such excessive length reduction during the annealing process leads to a low energy state made by micro-cracks (smaller than 1 mm), which are not necessarily correlated with the other fractures. To overcome this problem, the algorithm is constrained by fracture areal density, i.e. fracture length may decrease until the total summation of fracture lengths over the simulation area is not lower than the calculated areal density. Before length perturbation in each iteration, the algorithm checks the limitation, i.e. $\sum \frac{l}{A} > AD$. If it satisfies, the length changes unconditionally; but, if does not hold, it may only increase. This procedure regards the desired density while leaving orientation and position to be completely correlated without limiting length variations.

The object-based model introduced by Masihi and King does not incorporate the media heterogeneity (Masihi and King, 2007). Also, the implementation of non-constrained SA in the mentioned model results in the occurrence of some uncorrelated small fractures required to be omitted, which makes the simulation very time consuming. In this manner, the medium is subdivided into 7 layers and 10 vertical zones due to geologic and geomechanical heterogeneities, and the desired properties are assigned to each grid. This technique makes it possible to comprise all the possible changes in the media for more reliable modeling. The simulation resolution and also the time of ordinary grid-based method strongly depend on the number of grids; therefore, a better resolution is more time consuming. However, in the combinatorial scheme, simulation time only depends on the number of objects and grids that only possess the desired properties. In addition, the model calculations are performed in the entire media rather than separately in each grid. Consequently, the model supports not only the quantitative properties of fractures like shape and distribution, but also the qualitative properties of each grid, and is able to cope with even small changes in the media.

This manuscript exclusively discusses the density of fractures as the main reason for geologic and geomechanical heterogeneity. Firstly, rock mechanics parameters are assigned to the geologic layers as discussed above. Afterwards, fracture density constrains are defined deterministically in the well locations (as shown in Table 1) and a linear transition is assumed between them in each layer. Finally, the applicability of the proposed method for conditioning the object-based model with heterogeneous data is investigated.

b. Weighted energy calculation

Fractures are able to be displaced unconditionally in the medium during the simulation. In each grid, they are constrained by the corresponding density limitation, which results in the distribution of fractures due to grid density. Larger fractures occur in high density zones whereas the small ones happen in low density areas. Fractures as shown in apollonian shape filling algorithm by Mandelbrot tend to locate as far as possible from each other due to their size, which is also corroborated by the parameter r of the objective function of Equation 12 (Mandelbrot, 1982). In real cases, stress shadow around fractures affects their distance. Bour and Davy proposed a power law scaling for fracture distance of length l to the nearest fracture, i.e. l^m, where m is in the close interval of [0, 1] (Bour and Davy, 1999).

Therefore, fractures (especially large ones) do not accumulate in high density zones. They prefer to distribute with maximum distance with respect to each other and also a minimum length to decrease the energy. As a result, fractures may migrate to low density layers where their length is permitted to be reduced in the annealing process. It means that low density zones experience higher intensity and vice versa. To control such migrations, the energy function is multiplied by the inverse of the fracture

intensity of each grid. It must be noted that the multiplier of the layers or grids with no fractures is assumed to be equal to 10 (or any numbers larger than the others). This modification causes reverse migration to high density zones to satisfy the presence of large fractures in high density zones and the small ones in low density areas.

3. Results and discussion

The simulation is conducted with an initial temperature of 1,000,000 with a 3% decrease per each *T*-step. the modeling area is subdivided to 70 grids (7 vertical and 10 in *x*-direction) to incorporate the heterogeneities in both directions. The results are presented in Figure 3 after 725 temperature steps (over 3.4×10^6 iterative perturbations) to reach the thermal equilibrium, i.e. an acceptance ratio about 1 percent. An initial increase in energy is because of length enlargement (up to 90 m) in high density zones due to the constrained simulation related to layer 7 in Well #1 and layers 2 and 5 in Well #2. Fortunately, the assumption of linear lateral density variation is completely supported by the model and constrains are satisfied as shown in Figure 4.

Furthermore, the average length of fractures from the simulation, namely about 56.5 m, is verified by data of the well test (Figure 5-a). On the other hand, the orientation of the simulated fracture sets, which is about 15.4 and -74.6 degrees in the Cartesian coordinate system, is in good agreement with the dip angle of deterministic fractures measured by FMI (Figure 5-b).

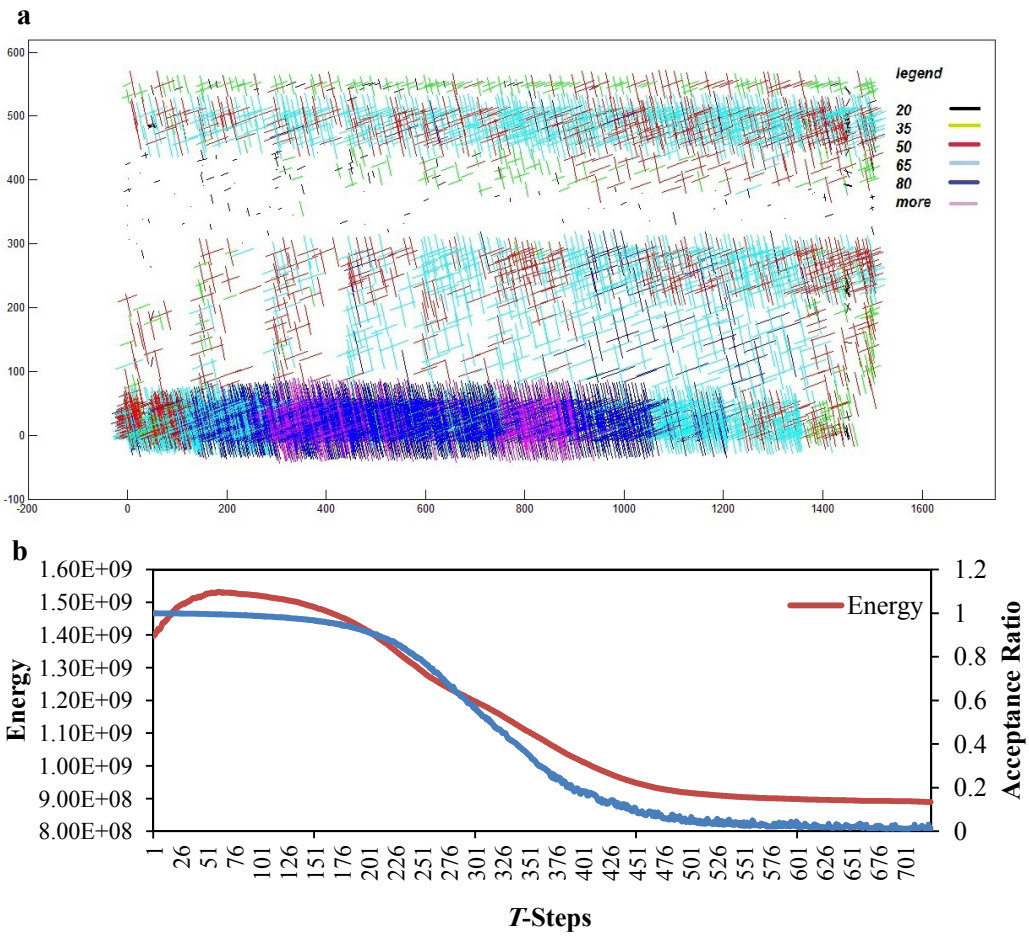

Figure 3

Realization of 5000 fracture networks: a) the distribution of fractures due to their location and length respect to desired densities; b) the plot of energy and acceptance ratio versus *T*-steps; the initial increase is the response of length increasing to adopt the model with the applied constrains; convergence is reached through 725 steps.

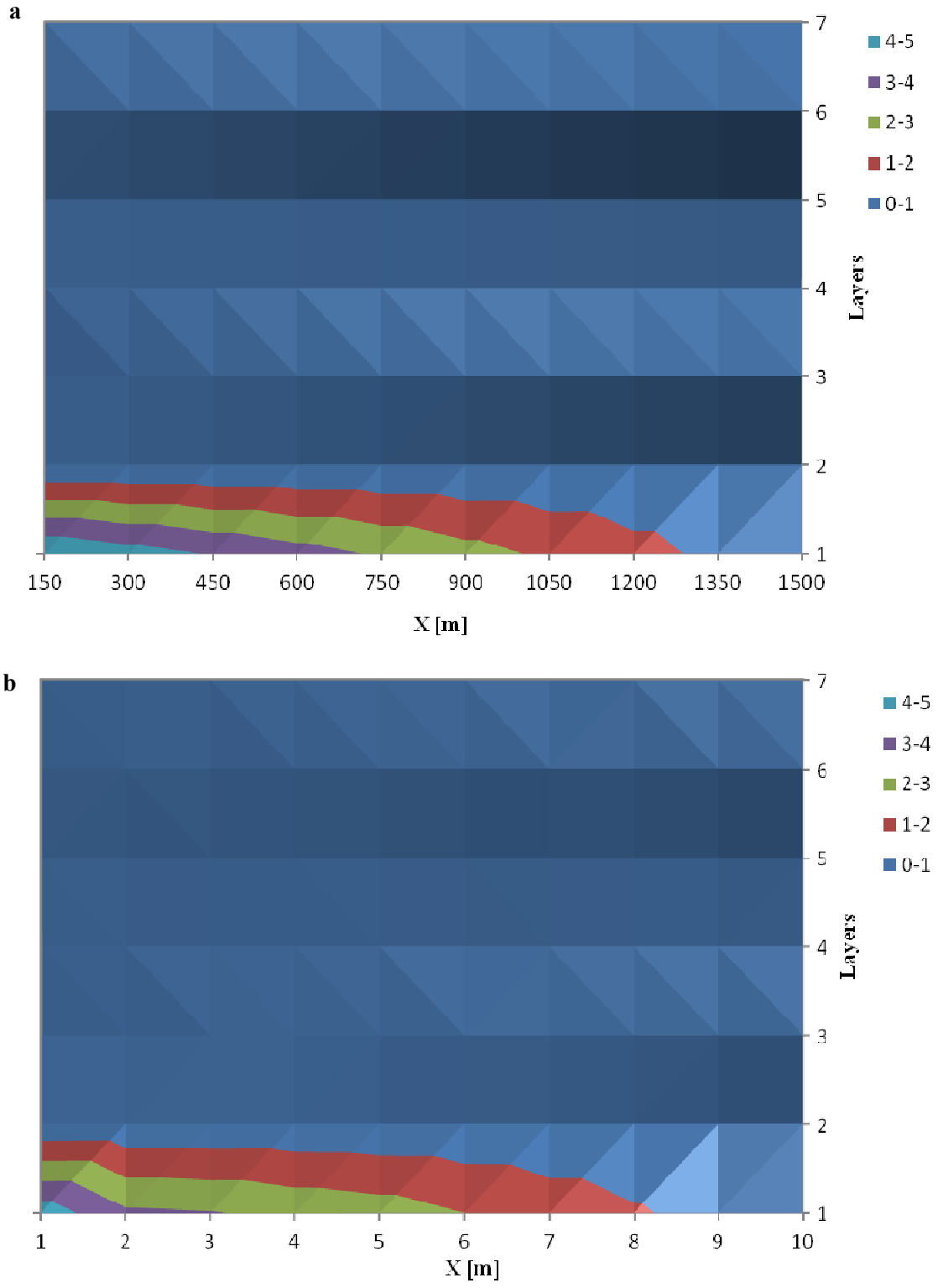

Figure 4
2D areal density variation; the satisfaction of vertical constrains and linear variation: a) conceptual model; b) simulation outputs.

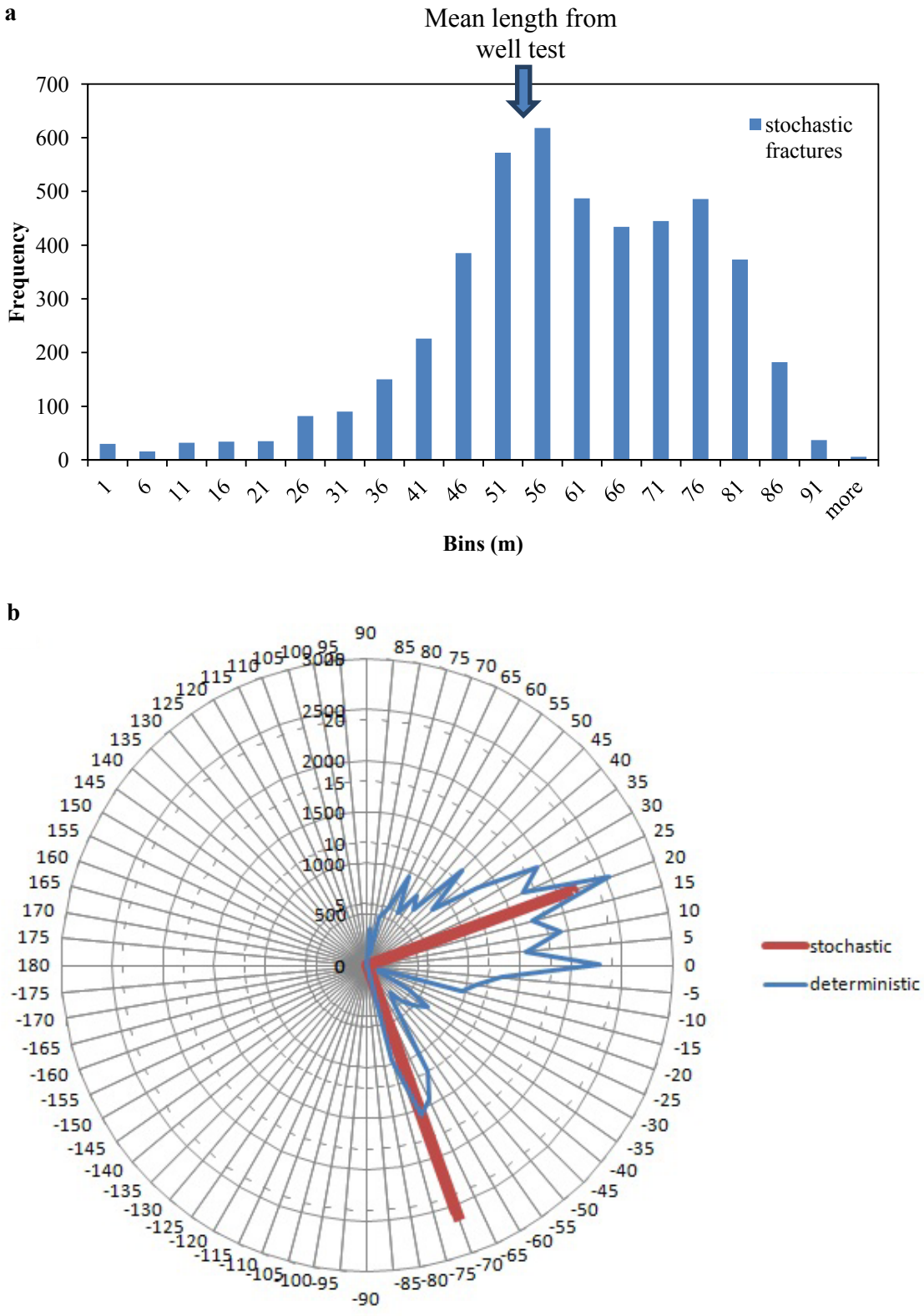

Figure 5
a) Histogram of stochastic fracture length satisfying well test mean length; b) orientation of stochastic fractures follows wellbore fracture dip angle

4. Conclusions

This current work presents a discrete fractures network model based on the strain displacement vectors for fracture network modeling. The model applies SA to optimize the spatial correlations of fractures for generating realizations of network by assuming that the energy follows Boltzmann distribution. A comprehensive heterogeneity study on rock mechanics parameters, fracture intensity, and areal density is also carried out to modify the algorithm to be conditioned with real data considering heterogeneity. To satisfy the desired constrains and control the unwanted migration of fractures toward low density zones, weighted energy calculation with respect to the inverse of fracture intensity is shown to be applicable.

Good agreement of the simulation results with experimental data demonstrates that conditioning the object-based model with heterogeneous data is feasible by means of gridding technique and constrained simulated annealing. This method is applicable to comprehensive fracture modeling on a field scale under wide heterogeneity conditions.

Acknowledgment

Authors would like to appreciate NISOC for supporting this research on novel methods in stochastic fracture modeling.

Nomenclature

DTC	: DSI compressional wave transit time
DTS	: DSI shear wave transit time
E	: Energy
E_{ij}	: Inelastic strain tensor
e_{ij}	: Strain tensor
FMI	: Formation microimager
l	: Length of fracture
L_{kl}	: Inverse of the Green's function
n	: Families of fissures plane
r	: Location vector
r_{ij}	: Distance vector
r_m	: Characteristics size of matrix block
S_{ij}	: Inelastic stress tensor
T	: Temperature
u	: Displacement vector
α	: Orientation of distance vector
δ	: Kronecker delta
θ	: Orientation of fracture
λ_{ijal}	: Standard isotropic elasticity tensor
μ	: Shear modulus
v	: Poisson's ratio
ρ_b	: Bulk density
σ_{ij}	: Stress tensor

References

Aarts, E. and Korst, J., Simulated Annealing and Boltzmann Machines: A Stochastic Approach to

Combinational Optimization and Neural Computing, 272 p., John Wiley, New York, 1989

Bear, J., Tsang, C. F., and de Marsily, G., Flow and Contaminant Transport in Fractured Rock, Academic Press, Inc., San Diego, CA, p. 169-231, 1993

Belani A. K., Jalai, Y., Estimation of Matrix Block Size Distribution in Naturally Fractured Reservoirs, Paper SPE 18171 Presented at the 63 Rd Annual Technical Conference and Exhibition of the Society of Petroleum Engineers Held in Houston, TX, October 2-5, 1988

Bour, O. and P. Davy, Clustering and Size Distributions of Fault Pattern: Theory and Measurements, Geophys. Res. Lett., Vol. 26, No. 13, p. 2001-2004, 1999

Bourdet D., Well Test Analysis: The Use of Advanced Interpretation Models, Elsevier, Amsterdam, Netherlands, p. 117-120, 2002

Daly, C., Stochastic Vector and Tensor Fields Applied to Strain Modeling, Pet. Geosci., Vol. 7, S97-S104, 2001

Deutsch C. V., Geostatistical Reservoir Modeling, Oxford University Press Inc, New York, Chapter 9, 2002

Engelder, T. and Peacock, D. C. P., Joint Development Normal to Regional Compression during Flexural-flow Folding: the Lilstock Buttress Anticline, Somerset, England, J. Struct. Geol., Vol. 23, p. 259-277, 2001

Guardiano, F., Srivastava, R., Multivariate Geostatistics: Beyond Bivariate Moments, Geostatistics-Troia, Kluwer Academic Publications, p. 133-144, 1993

Heffer, K. J., and King, P. R., Spatial Scaling of Effective Modulus and Correlation of Deformation Near the Critical Point of Fracturing, Pure Appl. Geophys., Vol. 163, No. 10, p. 2223-2242, 2006

Kirkpatrick, S., Gelatt, C. D., and Vecchi, M. P., Optimization by Simulated Annealing, Science, Vol. 220, p. 671-680, 1983

Kjetil M., Hals, D., and Berre, I., Interaction between Injection Points During Hydraulic Fracturing, Water Resources Research, Vol. 48, No. 11, p. WR012265, 2012

Landau, L. D., and Lifshitz, E. M., Theory of Elasticity, Course Theoret. Phys., Vol. 7, 134 p., Pergamum, London., 1959

Mandelbrot, B. B., The Fractal Geometry of Nature, 468 p., W. H. Freeman, New York, 1982

Masihi M., Sobhani M., Al-Ajmi A., Al-Wahaibi Y., and Al-Wahaibi T., A physically-based Three Dimensional Fracture Network Modeling Technique, Scientia Iranica, 2012, Vol. 19, No. 3, p. 594-604, 2012

Masihi, M., and King, P. R., A Correlated Fracture Network: Modeling and Percolation Properties, Water Resour. Res., Vol. 43, W07439, doi: 10.1029/2006WR005331, p. W07439, 2007

Metropolis. A., Rosebluth, M., Rosebluth, A., Teller, E., and Teller, J., Equations of State Calculations by Fast Computing Machine, J. Chem. Phys., Vol. 21, No. 6, p. 1087-1092, 1953

Priest, S. D., Discontinuity Analysis for Rock Engineering, 1st Ed., Chapman and Hall, London, 473 p., 1993

Ruhland, R., Méthode d'étude de la Fracturation Naturelle des Roches, Associé a Divers Modeles Structuraux. Geol. Soc. Bull., Vol. 26, No. 2-3, Strasbourg, 1973

Serra O., Fundamentals of Well Log Interpretation: the Acquisition of Logging Data, Elsevier, p. 235-237, 1986

Shekhar R. and Gibson R. L., Correlated Fracture Network Modeling Using Simulated Annealing, SEG Las Vegas 2008 Annual Meeting, 2008

Shekhar R., Gibson R. L., Generation of Spatially Correlated Fracture Models for Seismic Simulations, Geophys. J. Int., 185, p. 341-351, doi: 10.1111/j.1365-246X.2011.04937.x, 2011

Singhal, B. B. S., and Gupta R. P., Applied Hydrology of Fractured Rocks, Springer, 408 p, Chapter 2, 2010

Terzaghi, R. D., Sources of Error in Joint Surveys. Geotechnique, Vol. 15, p. 287-304, 1965

Tran, N. H., Chen, Z. X., and Rahman, S. S., Integrated Conditional Global Optimization for Discrete Fracture Network Modeling, Comput. Geosci., Vol. 32, p. 17-27, 2006

Tran, N. H., Simulated Annealing Technique in Discrete Fracture Network Inversion: Optimizing the Optimization, Comput. Geosci., Vol. 11, p. 249-260, 2007

Warren, J. E. and Root, P. J., Behavior of Naturally Fractured Reservoirs, Soc. Pet. Eng. J., p. 245-255, 1963